Research Article | Vol. 32, No. 22 / 21 Oct 2024 / Optics Express 39974
Optics EXPRESS

Modulation bandwidth analysis of GaN-based micro-LED deduced by an equivalent circuit model

LINGLI ZHU,[1] ZHEN ZHANG,[2] DAQI SHEN,[2] NA GAO,[1,3] PENGFEI TIAN,[2,4] SHUPING LI,[1] JUNYONG KANG,[1,5] AND RONG ZHANG[1]

[1]*Fujian Key Laboratory of Semiconductor Materials and Applications, College of Physical Science and Technology, Xiamen University, Xiamen 361005, China*
[2]*Institute for Electric Light Sources, School of Information Science and Technology, Fudan University, Shanghai 200433, China*
[3]*ngao@xmu.edu.cn*
[4]*pftian@fudan.edu.cn*
[5]*jykang@xmu.edu.cn*

Abstract: We establish an equivalent circuit model of the GaN-based micro-LED system incorporating the parasitic parameters of the printed circuit board and bonding wires. Our deep analysis reveals that the parameters of intrinsic micro-LED significantly impact the modulation bandwidth of micro-LED. As the resistance and capacitance of micro-LED increases, the bandwidth of micro-LED decreases sharply. To address this critical issue, we propose several feasible strategies based on the analysis of the equivalent circuit model. In particular, we develop deep etching techniques to improve the bandwidth of the micro-LED system. By fitting the impedance parameters of the equivalent circuit model of shallow and deep etching micro-LEDs, the electrode capacitance of the deep-etching device is decreased by 24.9 pF compared to the shallow-etching device. This leads to a remarkable modulation bandwidth enhancement from 203 MHz to 249.8 MHz at a low current density of 4 kA/cm^2. The high consistency of the simulated bandwidth from fitted parameters proves the validation and reliability of our proposed equivalent circuit model.

1. Introduction

To deeply serve the physical world, the visioning and planning of sixth-generation (6 G) communications are highly expected to support applications in accurate indoor positioning, vertical industries, worldwide connectivity and integrated networking, etc [1]. However, conventional electronic technologies face enormous challenges hindered by spectrum congestion, *i.e.*, a traffic jam in the radio frequency spectrum, which significantly restricts the realization of high data rate, security, and secrecy features of 6 G [2,3]. Recently, the emergence of optical wireless communication via the new technology of visible light communications has been considered a solution to the critical issues in 6 G regarding high data rate, coverage, and enhanced security [4]. Therefore, the widespread use of GaN-based LEDs plays a crucial role in the rise of visible light communications [5]. Driven by the premise of the above application scenarios, the bandwidth of LED is a critical factor in determining the data rate and transmission; the broader the modulation bandwidth, the more robust the ability to transmit data and signals [5–7]. Recent research on micro-LEDs with dimensions smaller than 100 μm has demonstrated excellent ability in a broader bandwidth due to the small RC time constants and reduced differential carrier lifetimes compared to conventional LEDs [8–11]. Moreover, recent research has also explored numerous strategies to enhance the modulation bandwidth of GaN-based micro-LEDs. For example, Arman Rashidi *et al.* have designed a micro-LED of 60 μm grown on a nonpolar

#539321 https://doi.org/10.1364/OE.539321
Journal © 2024 Received 13 Aug 2024; revised 4 Oct 2024; accepted 7 Oct 2024; published 17 Oct 2024

Optics EXPRESS

GaN substrate to achieve a high modulation bandwidth of 524 MHz at a current density of 10 kA/cm^2 [12]. Guo *et al.* have increased the modulation bandwidth from 174 MHz to 380 MHz by reducing the mesa size from 120 µm to 60 µm [13]. Additionally, by employing the localized surface plasmon resonance of Al nano-triangle arrays, Zhang *et al.* have improved the bandwidth of 6×6 deep-ultraviolet micro-LED arrays of 100 µm from 180 MHz to 300 MHz at a current density of 200 A/cm^2 [14].

Despite advancements in GaN-based micro-LED bandwidth, most efforts to improve modulation bandwidth are attributed to the decreased RC constant and the reduction of carrier lifetimes based on the ABC model [15–18]. On the one hand, directly measuring the carrier lifetimes is complicated. On the other hand, the capacitance of micro-LED needs to be conducted at a specific frequency that neglects the parasitic inductance within it and cannot be applied across the entire frequency spectrum [19]. Herein, the equivalent circuit model has promising advantages for the quantitative analysis of modulation bandwidth to eliminate measuring carrier lifetimes. Moreover, the equivalent circuit model considers the effect of capacitance and inductance, allowing it to be applied over a broader frequency range. In 1975, T. P. Lee initially proposed the small-signal equivalent model to analyze the impact of space charge capacitance on the turn-on delay of the laser diode [20]. This model has been widely used over the past decades to minimize the impact of parasitic effects on the chip response in vertical-cavity surface-emitting lasers and micro-LEDs to determine their intrinsic bandwidth [21–24]. Recently, Xicong Li *et al.* have investigated the impedance and bandwidth of commercial diodes under encapsulation and electrostatic discharge conditions based on the small-signal equivalent model [25]. However, a quantitative analysis of the impedance properties of the micro-LED circuit and its impact on modulation bandwidth at high frequencies remains when packaging is taken into account. The quantitative effects of each element within the circuit of the equivalent small-signal model on impedance and bandwidth are currently unknown. Therefore, establishing a small-signal equivalent circuit model for the micro-LED system will facilitate designing drivers or modulators and enable superior impedance matching while revealing the origins and effects of undesired elements.

In this work, we constructed an equivalent circuit model of GaN-based micro-LED systems that incorporates the parasitics of the printed circuit board (PCB) and the bonding wires. To ensure practical relevance, we first calculated the equivalently operating range for each parameter and examined its quantitative impact on the impedance and modulation bandwidth of the micro-LED circuit, respectively. Using the modified equivalent model, we have proposed several strategies, including the deep-etching strategy, to improve the bandwidth of micro-LEDs. By fitting the impedance values obtained from two different micro-LED devices (via shallow and deep etching processes) into the circuit model parameters, we compared the simulated and measured modulation bandwidth and found an enhancement of deep etching designs, validating the practicality of our established model. This study has significant implications for designing and optimizing micro-LED systems, particularly in providing a fundamental reference for realizing broader bandwidth micro-LED communication systems.

2. Small-signal circuit model

Figure 1(a) displays the equivalent circuit of a complete micro-LED system, which includes the intrinsic equivalent circuit of the micro-LED, the bonding wire, and the packaging circuit. Figure 1(b) presents a picture and schematic diagram of the micro-LED system and equivalent details that will be further discussed in the following sections. We proceeded to calculate the approximate values of the main parasitics for each RLC (resistance, inductance and capacitance) parameter in the circuit. Using the tuning function in advanced design system software, we further adjusted the parameters within a broad range and ultimately obtained precise values.

Optics EXPRESS

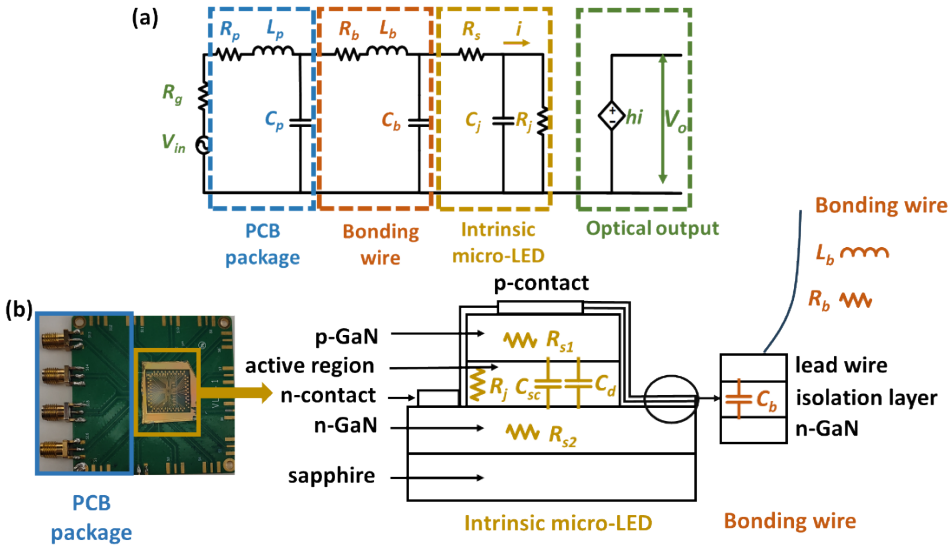

Fig. 1. (a) Equivalent model circuit of the micro-LED system. (b) Picture and equivalent diagram of the micro-LED and the bonding wire.

2.1. *Intrinsic micro-LED*

According to the previous study, the derived frequency response of active region in micro-LED is analogous to that of a single-pole parallel *RC* circuit [26]. Consequently, we regard the active region of micro-LED as a parallel *RC* circuit.

Subsequently, we determine the actual resistance and capacitance values within the micro-LED for the equivalent circuit. Derived from the voltage-current tests, the gradient of the voltage-current relationship of the micro-LED is utilized to define the actual resistive value of the equivalent circuit model. The equivalent capacitance of the active region in intrinsic micro-LED C_j is then achieved by fitting the *S11* parameter. This capacitance C_j in the micro-LED represents the sum of the space charge capacitance C_{sc} and the diffusion capacitance C_d [25,27,28].

Moreover, a complete micro-LED with metal connections also introduces a certain amount of series resistance. This includes resistance from Ohmic contacts, current crowding beneath the electrodes, metal lead wire, and all micro-LED parts outside the active region [8]. These resistances, collectively called series resistance R_s, are crucial in understanding the impedance value under direct current.

2.2. *Bonding wire*

Encapsulating discrete micro-LED chips is imperative to testing and practical application. Different encapsulation methods can introduce varying parasitic parameters. Here, we utilize a printed circuit board connection, where the PCB is linked to the micro-LED with gold wire bonding. Therefore, a series of parasitic parameters are introduced due to the bonding wires, including electrode capacitance C_b, parasitic inductance L_b, and parasitic resistance R_b.

To ensure the accuracy of the equivalent model parameters, the resistance and inductance of the bonding wires have been calculated based on the relevant formulas, serving as a reference range for the equivalent resistance and inductance of the packaging and bonding. The equivalent resistance of the bonding wire is calculated as following:

$$R = \rho \frac{L}{s}, \tag{1}$$

Optics EXPRESS

Here, ρ represents the resistivity of the metal wire, L denotes the length of the metal wire, and s signifies the cross-sectional area of the metal wire. The inductance of the bonding wire is divided into self-inductance and mutual inductance. The self-inductance is calculated according to the formula [29]:

$$L = 5d\left(n\frac{2d}{r} - \frac{3}{4}\right), \tag{2}$$

Moreover, the mutual inductance is calculated according to the formula [29]:

$$L = 5d\left\{ln\frac{2d}{s} - 1 + \frac{s}{d} - \left(\frac{s}{2d}\right)^2\right\}, \tag{3}$$

where r represents the radius of the wire, d denotes the length of the wire, and s signifies the center-to-center distance between two wires. Substituting the gold wire with a radius of 25 μm, a resistivity of 2.01 μΩ/cm, assuming a length of 1 cm for the bonding wire, and a center-to-center distance of 0.5 cm between the two cylindrical wires. Ultimately, the resistance is determined to be 0.408 Ω. The self-inductance, mutual inductance, and total inductance are 13.01 nH, 2.43 nH, and 10.58 nH, respectively.

2.3. PCB packaging

In addition to the impacts of the bonding wires, the PCB packaging itself introduces certain parasitic capacitance C_p and inductance L_p. The soldering process contributes an additional resistive R_p. Through testing (Keithley 4200A), the parasitic capacitance of the PCB is confirmed to be 4 pF, the parasitic inductance is 2 nH, and R_p is derived by fitting the *S11* curve.

2.4. Integrated circuit model

Taking all the elements into account, we can achieve the integrated equivalent circuit shown in Fig. 1(a). Thus, the expression for the equivalent circuit impedance of the micro-LED can be formulated as follows:

$$Z_{micro-LED} = R_p + j\omega L_p + \frac{1}{j\omega C_p} \,//\, \left(R_b + j\omega L_b + \frac{1}{j\omega C_b} \,//\, \left(R_s + \frac{1}{j\omega C_j} \,//\, R_j\right)\right), \tag{4}$$

where ω denotes the angular frequency. The transfer function of micro-LED can be calculated using the following equation:

$$\begin{aligned} H(\omega)_{micro-LED} &= \frac{V_o}{V_{in}} = \frac{hi}{V_{in}} = \frac{h}{R_j}\frac{V_{R_j}}{V_{in}} \\ &= \frac{h}{R_j}\frac{\frac{1}{j\omega C_j} \,//\, R_j}{R_p + j\omega L_p + \frac{1}{j\omega C_p} \,//\, (R_b + j\omega L_b + \frac{1}{j\omega C_b} \,//\, \left(R_s + \frac{1}{j\omega C_j} \,//\, R_j\right))} \end{aligned}, \tag{5}$$

This equation is so complicated that it is challenging to discern the impact of each variable on $H(\omega)_{micro-LED}$. To better understand the mechanisms of how these parameters affect the bandwidth, the intrinsic micro-LED equivalent circuit shown in Fig. 1(a) can be further expressed as follows:

$$H(\omega)_{micro-LED} = \frac{I_{out}}{I_{in}} = \frac{\frac{1}{j\omega C_j}}{\frac{1}{j\omega C_j} + R_j} = \frac{1}{1 + j\omega C_j R_j}, \tag{6}$$

Furthermore, the amplitude-frequency response is following:

$$|H(\omega)_{micro-LED}| = \left|\frac{1}{1 + j\omega C_j R_j}\right| = \frac{1}{\sqrt{1 + (\omega C_j R_j)^2}}, \tag{7}$$

where the -3 dB bandwidth equals to $\frac{1}{2\pi C_j R_j}$. $H(\omega)_{micro-LED}$ aligns perfectly with the expression of previous study [26], further confirming the intrinsic equivalent circuit of the micro-LED

Optics EXPRESS

depicted in Fig. 1(a). Keeping the capacitance and frequency constant, the larger the resistance, the smaller the value of $H(\omega)$, and the corresponding bandwidth is reduced. Similarly, when the resistance and frequency are constant, the larger the capacitance, the smaller the $H(\omega)$, and the corresponding bandwidth is also decreased. Furthermore, the intrinsic micro-LED can be considered as a $Z_{micro-LED}$ when examining the bandwidth of bonding wire, similar to an *RC* parallel circuit. When assessing the bandwidth of the PCB, the bonding wire and the micro-LED can also be regarded as Z_B, which is equivalent to analyzing the bandwidth of an *RC* parallel circuit.

3. Experimental details

A GaN-based green LED was grown on a *c*-plane sapphire substrate using metal-organic chemical vapor deposition (MOCVD) technology. The LED structure is comprised of an unintentionally doped layer, *n*-type GaN, a superlattice layer, a multi-quantum well layer, an electron blocking layer, a *p*-type GaN layer, and an indium tin oxide (ITO) layer in sequence from bottom to up. Through a series of standard processes of plasma-enhanced chemical vapor deposition (PECVD), photolithography, inductively coupled plasma etching, and magnetron sputtering, two types of micro-LED structures were fabricated. The two type devices, each with a specific depth, were achieved by shallow-etched (SE, common *n* electrodes) above the *n*-type GaN and deep-etched (DE, non-common *n* electrodes) down to the sapphire substrate.

Figures 2(a) and (b) show the cross-sectional schematic structures of the two micro-LED devices. The mesa size of the micro-LED is 40 µm. A 300 nm silicon dioxide layer was deposited as an insulating barrier on the 40 nm ITO layer by PECVD. The *p*-type and *n*-type GaN were interconnected with a conductive 50/250/50/200 nm Ti/Al/Ti/Au film through the holes in this silicon dioxide layer. Finally, both devices were annealed at 550 °C in an N_2 atmosphere for ten minutes to form Ohmic contact.

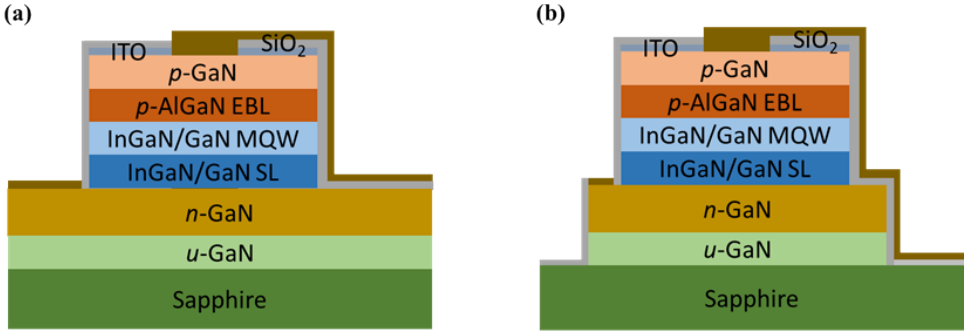

Fig. 2. (a) Schematic cross-sectional diagrams of the shallow etching (SE) and (b) deep etching (DE) structures.

Based on the fabricated GaN-based micro-LEDs, we use gold bonding wires to connect the device to the PCB. The testing system consists of a micro-LED, two lenses, a photodetector (Femto 1.4 G PIN), and a network analyzer (Agilent, N5225 A, 10 MHz-50 GHz). The AC signal from the network analyzer and the DC signal from the power supply is modulated through a bias-Tee before being charged into the micro-LED. The emitted light from the micro-LED passes through two lenses and is collected by a photodetector. The photodetector then converts the optical signals into electrical signals, which are transmitted to the network for analysis of the equivalent input return loss *S11* and the forward transmission coefficient *S21*. All of the measurements were carried out at room temperature. We can determine the impedance through the *S11* and the bandwidth through the *S21* for the integrated circuit. The frequency of the

Optics EXPRESS

network analyzer signals ranges from 10 MHz to 2 GHz, and the specific circuit connection has been described in our previous work [30]. The tested results will be discussed in Fig. 6.

4. Results and discussion

To analyze how each parameter affects the impedance and bandwidth of the micro-LED system, we define the RLC parameters calculated from the constructed circuit model process $R_p = 5\ \Omega$, $R_b = 4.35\ \Omega$, $R_s = 5\ \Omega$, $R_j = 110\ \Omega$, $L_p = 2.3$ nH, $L_b = 14$ nH, $C_p = 4.8$ pF, $C_b = 4$ pF, $C_j = 55$ pF as a reference. We then use the controlled variable method to qualitatively observe the effect of each parameter on impedance and bandwidth. Figure 3 illustrates the impact of RLC parameters on *S11*. Notably, the curve spans from the inner to the outer parts as the network analyzer frequency increases from 10 MHz to 2 GHz. Under the frequency of 10 MHz to 2 GHz, the *S11* varies significantly with the varying PCB parameters of R_p, L_p, and C_p (R_p: 5~180 Ω, L_p: 2.3~180 nH, C_p: 4.8~180 pF), as shown in Figs. 3(a), (b), and (c). In Figs. 3(d), (e), and (f), *S11* exhibits substantial changes at the frequency of 10 MHz to 1 GHz with increased R_b, L_b, and C_b parameters of bonding wires while changing minimally at 1~2 GHz. However, the *S11* varies less at a frequency of 600 MHz to 2 GHz while increasing R_s, R_j, and C_j (R_s: 5~180 Ω, R_j: 10~200 Ω, C_j: 5~200 pF) of the intrinsic micro-LED circuit in Figs. 3(g), (h), and (i). The impact of R_j and C_j on *S11* at a frequency of 10~600 MHz is greater than at higher frequencies. This is because the capacitor preferentially passes through the high-frequency signals. Thus, as current flows directly through the C_p at relatively high frequencies, the influence of micro-LED and bonding wires can be ignored for the impedance of the equivalent circuit. However, as the frequency decreases to a threshold, the capacitor impedance gradually increases, which leads to a current division based on the impedance values of the capacitors C_p, micro-LED, and bonding wires. The selected RLC parameters determine the threshold frequency behaviors of the equivalent circuit. Therefore, the RLC parameters of the micro-LED, bonding wires, and PCB are favorable to fit *S11* at a frequency of 10~ 600 MHz, 600 MHz~1 GHz, and 1~2 GHz, respectively.

As previously mentioned, the *S21* parameter is crucial for determining the modulation bandwidth of the micro-LEDs. Using the controlled variable method, we analyzed the variation of *S21* versus different parameters in Fig. 4. The bandwidth is defined as the value of the *S21* parameter dropping to -3 dB. It can be observed that *S21* gradually decreases as the resistance increases. However, the curves show less change at a frequency of 200 MHz, with a difference of approximately 2 dB when varying R_p, R_b, and R_s in Figs. 4(a), (d) and (g). On the other hand, the impact of R_j on the S21 is more pronounced in Fig. 4(h) when increased from 10 Ω to 200 Ω. Similarly, the *S21* experiences a significant drop with the increased capacitance C_j in Fig. 4(i). This shows that the parameters of the PCB have a weaker impact compared to those of the bonding wires, and both are less significant than the parameters of intrinsic micro-LEDs.

Figure 5(a-c) depicts the relationship between the -3 dB bandwidth of *S21* and the varying RLC parameters of the equivalent circuit. As the resistance increases, the bandwidth gradually decreases. On the one hand, the parallel capacitance associated with R_b and R_s is relatively slight. Thus, the product of their values is comparatively tiny compared to the change of frequency, leading to a trifling alteration in the bandwidth concerning R_b and R_s. On the other hand, R_p R_b and R_s are in series with the subsequent $Z_{micro-LED}$ or Z_b, and the equivalent resistance of the micro-LED is considerably larger than resistances of R_p and R_b, which causes the increase of these resistances to be diluted by the series-connected $Z_{micro-LED}$ or Z_b; therefore, variations in R_p, R_b, and R_s have a negligible impact on the bandwidth, but the impact of R_j on the bandwidth is significant. The connection and properties of the inductor are similar to those of the resistor. As the inductance increases, it counteracts the capacitive reactance, improving the bandwidth. However, as the inductance continues to increase, the impact of the inductive reactance is more significant, and the bandwidth tends to decrease. The impact of C_j on the bandwidth is substantial, while the impacts of C_p and C_b are not significant. The capacitive reactance introduced by C_p

Optics EXPRESS

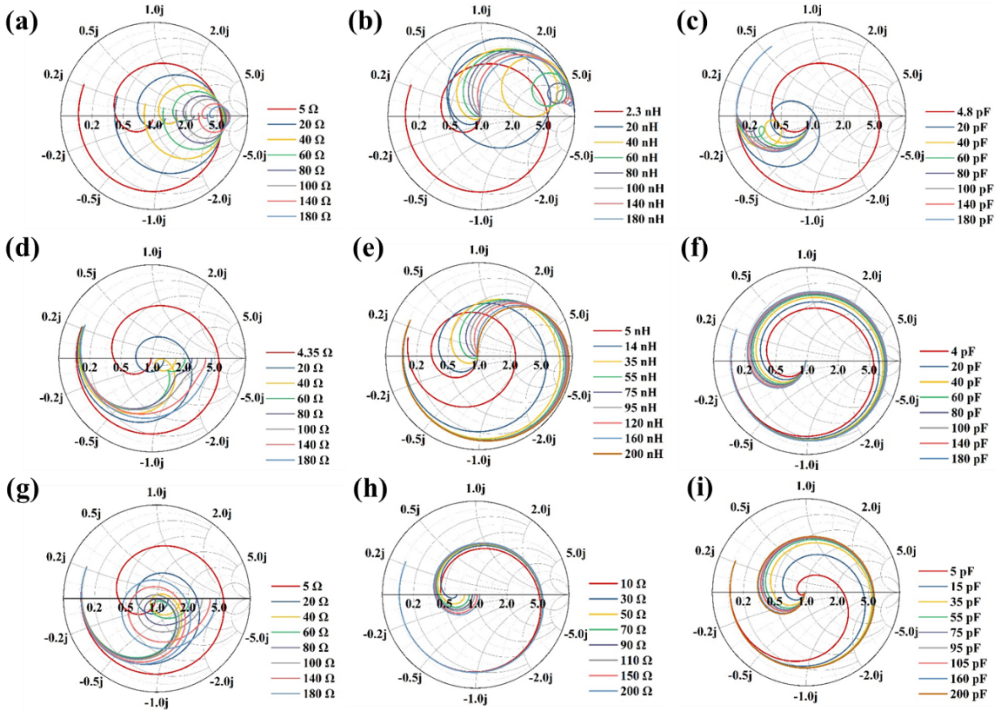

Fig. 3. Input return loss (*S11*) varies with the RLC parameters of PCB (a) R_p, (b) L_p, (c) C_p, and bonding wires (d) R_b, (e) L_b, (f) C_b, and intrinsic micro-LED (g) R_s, (h) R_j, (i) C_j.

and C_b is diluted by the capacitive reactance present in $Z_{micro-LED}$ or Z_b, enabling the decrease in bandwidth due to an increase in C_p and C_b less noticeable. However, the value of C_j is larger than C_p and C_b and is not affected by the capacitive reactance of the series-connected circuit in the subsequent stages. Thus, the increase in capacitance C_j has a more significant impact on the bandwidth reduction.

Based on the analysis of *S21*, we propose several strategies to improve the modulation bandwidth of the micro-LED system. One approach is to decrease the C_j, R_j, and R_s of micro-LEDs by minimizing the number of quantum wells or increasing the carrier concentration in the *p*-type layer. As mentioned in our previous work, the extremely thin quantum barrier is beneficial for enhancing the carrier recombination rate and shortening the radiative recombination carrier lifetime due to the reduced quantum confined Stark effect [31], thereby reducing R_j and C_j. Similarly, the decreased number of quantum wells will likely decrease R_j and C_j. The high hole concentration in *p*-type GaN can improve the electrical conductivity, thus lowering series resistance R_s. It is also possible to reduce C_b by decreasing the size of the *n*-electrode or *p*-electrode while changing the contact area through new manufacturing processes. Additionally, we can minimize the parasitic R_b and L_b of the bonding wires by reducing the length of the bonding wire or increasing the spacing between the bonding wires. Moreover, reducing the parasitic R_p, L_p, and C_p of the PCB is achievable. To validate the accuracy of the circuit model analysis, we have developed a deep etching method to fabricate micro-LEDs in addition to the usual shallow etching micro-LEDs.

Figure 6(a) displays the normalized *S21* simulated and measured curves. The measured modulation bandwidth is 203 MHz and 249.8 MHz for SE and DE micro-LEDs, while the simulated bandwidth is approximately 200 MHz and 260 MHz for SE and DE devices, respectively. The simulated values agree well with the experimental results, validating the accuracy of our

Optics EXPRESS

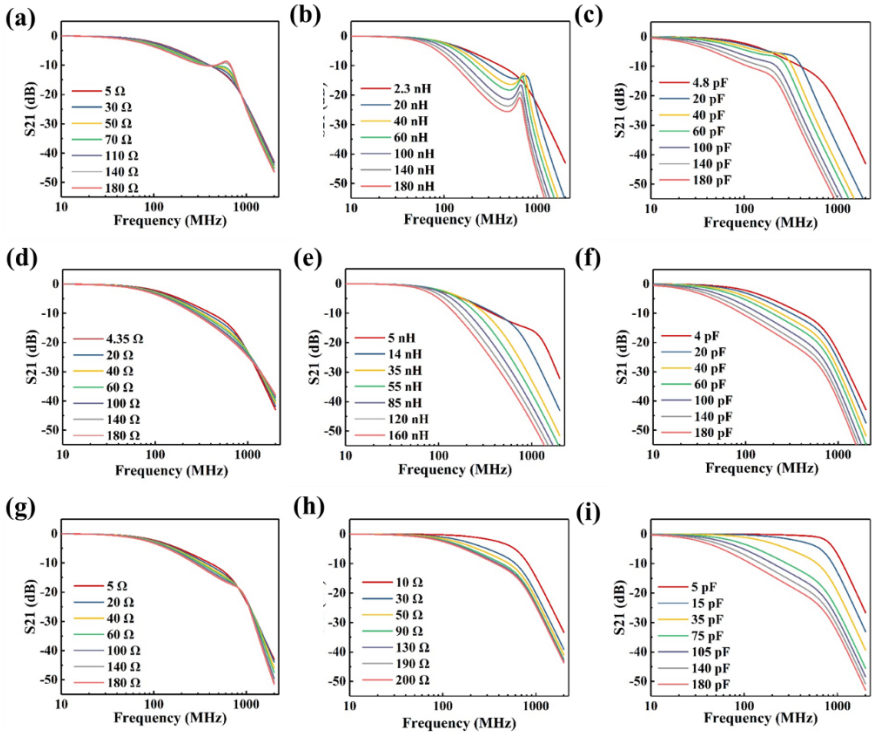

Fig. 4. Normalized forward transmission coefficient (*S21*) varies with the RLC parameters of PCB (a) R_p, (b) L_p, (c) C_p, and bonding wires (d) R_b, (e) L_b, (f) C_b, and intrinsic micro-LED (g) R_s, (h) R_j, (i) C_j.

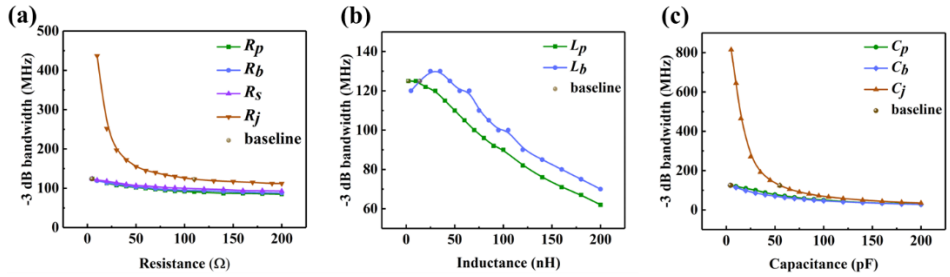

Fig. 5. Modulation bandwidth varies with different (a) R, (b) L, (c) C of the micro-LED system.

model. In Fig. 6(b) and Table 1, the impedance parameters of RLC in the equivalent circuit are further calculated using the *S11* of the established circuit model. The parameters R_p, L_p, and L_b show tiny changes induced by the welding process during the packaging and the length and spacing of the bonding wires of SE and DE chips. However, the difference for parameters R_s and C_b is larger. This is because of smaller contact area of electrodes in DE devices compared to SE n electrodes, leading to an increased resistance R_s. The variation in C_b is due to the creation of parallel-plate additional electrode capacitance, composed of n-GaN, isolation layer SiO_2 and leading wire in Fig. 1(b). Differing from the SE device, the DE process removes the n-type GaN, significantly reducing the electrode capacitance C_b, thereby increasing the bandwidth of micro-LED. This indicates the impact of DE process on the performance of micro-LEDs.

Optics EXPRESS

Table 1. Calculated RLC parameters for the SE and DE micro-LEDs based on the equivalent circuit model

	$R_p(\Omega)$	C_p(pF)	L_p(nH)	$R_b(\Omega)$	C_b(pF)	L_b(nH)	$R_s(\Omega)$	C_j(pF)	R_j(nH)
SE	1	4.8	2.3	4	25	14	17	34	24
DE	1.2	4.8	2.5	4	0.1	18	40.8	44	24

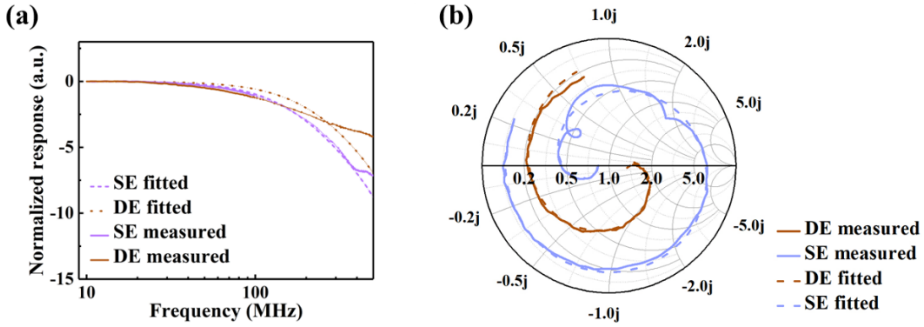

Fig. 6. (a) *S21* and (b) *S11* obtained from the equivalent circuit model of the simulated and experimental results.

5. Conclusion

In this work, we developed an equivalent circuit model of the GaN-based micro-LED system, considering the intrinsic micro-LED, bonding wires, and PCB packaging. Through a comprehensive analysis of the impacts on impedance and bandwidth, we identified several key strategies to enhance the modulation bandwidth of micro-LEDs. These strategies, which include reducing the C_j, R_j, and R_s of the micro-LED and minimizing the parasitic C_b, R_b, and L_b of the bonding wires, are significant as they pave the way for improved performance of micro-LED systems. We also proposed an effective strategy of using deep etching techniques instead of conventional shallow etching processes during the micro-LED fabrication to decrease C_b. By measuring the impedance and bandwidth of the two types of micro-LEDs with shallow and deep etching processes, we found that the electrode capacitance C_b of the deep-etching device is decreased by 24.9 pF. This led to a substantial enhancement in bandwidth from 203 MHz to 249.8 MHz at 4 kA/cm^2 current density. We believe this analytical method provides a fundamental scientific reference for effectively improving the bandwidth of micro-LED systems.

Funding. National Key Research and Development Program of China (2021YFB3600100); National Natural Science Foundation of China (62135013, 62234001, 62175203); Science and Technology Commission of Shanghai Municipality (No. 23ZR1405700).

Disclosures. The authors declare no conflicts of interest.

Data availability. Data underlying the results presented in this paper are not publicly available at this time but may be obtained from the authors upon reasonable request.

References

1. V. K. Quy, A. Chehri, N. M. Quy, *et al.*, "Innovative Trends in the 6 G Era: A Comprehensive Survey of Architecture, Applications, Technologies, and Challenges," IEEE Access **11**, 39824–39844 (2023).
2. S. Dang, O. Amin, B. Shihada, *et al.*, "What should 6 G be?" Nat. Electron. **3**(1), 20–29 (2020).
3. J. P. M. G. Linnartz, X. Deng, A. Alexeev, *et al.*, "Wireless Communication over an LED Channel," IEEE Commun. Mag. **58**(12), 77–82 (2020).
4. L. Grobe, A. Paraskevopoulos, J. Hilt, *et al.*, "High-speed visible light communication systems," IEEE Commun. Mag. **51**(12), 60–66 (2013).
5. R. Lin, X. Liu, G. Zhou, *et al.*, "InGaN Micro-LED Array Enabled Advanced Underwater Wireless Optical Communication and Underwater Charging," Adv. Opt. Mater. **9**(12), 2002211 (2021).

Optics EXPRESS

6. P. Qiu, S. Zhu, Z. Jin, *et al.*, "Beyond 25 Gbps optical wireless communication using wavelength division multiplexed LEDs and micro-LEDs," Opt. Lett. **47**(2), 317–320 (2022).
7. S. Rajbhandari, J. J. D. McKendry, J. Herrnsdorf, *et al.*, "A review of gallium nitride LEDs for multi-gigabit-per-second visible light data communications," Semicond. Sci. Technol. **32**(2), 023001 (2017).
8. A. Rashidi, M. Nami, M. Monavarian, *et al.*, "Differential carrier lifetime and transport effects in electrically injected III-nitride light-emitting diodes," J. Appl. Phys. **122**(3), 035706 (2017).
9. J. W. Shi, K. L. Chi, J. M. Wun, *et al.*, "III-Nitride-Based Cyan Light-Emitting Diodes With GHz Bandwidth for High-Speed Visible Light Communication," IEEE Electron Device Lett. **37**, 1 (2016).
10. R. X. G. Ferreira, E. Xie, J. J. D. McKendry, *et al.*, "High Bandwidth GaN-Based Micro-LEDs for Multi-Gb/s Visible Light Communications," IEEE Photon. Technol. Lett. **28**(19), 2023–2026 (2016).
11. J. W. Shi, J. K. Sheu, C. H. Chen, *et al.*, "High-Speed GaN-Based Green Light-Emitting Diodes With Partially n-Doped Active Layers and Current-Confined Apertures," IEEE Electron Device Lett. **29**(2), 158–160 (2008).
12. A. Rashidi, M. Monavarian, A. Aragon, *et al.*, "High-Speed Nonpolar InGaN/GaN LEDs for Visible-Light Communication," IEEE Photon. Technol. Lett. **29**(4), 381–384 (2017).
13. L. Guo, Y. Guo, J. Yang, *et al.*, "275 nm Deep Ultraviolet AlGaN-Based Micro-LED Arrays for Ultraviolet Communication," IEEE Photonics J. **14**(6), 1–8 (2022).
14. S. Zhang, R. He, Y. Duo, *et al.*, "Plasmon-enhanced deep ultraviolet Micro-LED arrays for solar-blind communications," Opt. Lett. **48**(15), 3841–3844 (2023).
15. Z. Li, X. Zhang, Z. Hao, *et al.*, "Bandwidth Analysis of High-Speed InGaN Micro-LEDs by an Equivalent Circuit Model," IEEE Electron Device Lett. **44**(5), 785–788 (2023).
16. F. Hu, S. Chen, G. Li, *et al.*, "Si-substrate LEDs with multiple superlattice interlayers for beyond 24Gbps visible light communication," Photonics Res. **9**(8), 1581–1591 (2021).
17. H. Chai, S. Yao, L. Lei, *et al.*, "High-Speed Parallel Micro-LED Arrays on Si Substrates Based on Via-Holes Structure for Visible Light Communication," IEEE Electron Device Lett. **43**(8), 1279–1282 (2022).
18. Z. Zhu, L. Lei, T. Lin, *et al.*, "Embedded Electrode Micro-LEDs With High Modulation Bandwidth for Visible Light Communication," IEEE Trans. Electron Devices **70**(2), 588–593 (2023).
19. X. Shan, G. Wang, S. Zhu, *et al.*, "Comparison of Beyond 1 GHz C-Plane Freestanding and Sapphire-Substrate GaN-Based micro-LEDs for High-Speed Visible Light Communication," J. Lightwave Technol. **41**(5), 1480–1486 (2023).
20. T. P. Lee, "Effect of junction capacitance on the rise time of led's and on the turn-on delay of injection lasers," The Bell Syst. Tech. J. **54**(1), 53–68 (1975).
21. A. Bacou, A. Hayat, V. Iakovlev, *et al.*, "Electrical Modeling of Long-Wavelength VCSELs for Intrinsic Parameters Extraction," IEEE J. Quantum Electron. **46**(3), 313–322 (2010).
22. A. Bacou, A. Hayat, A. Rissons, *et al.*, "VCSEL Intrinsic Response Extraction Using T-Matrix Formalism," IEEE Photon. Technol. Lett. **21**(14), 957–959 (2009).
23. I. Esquivias, S. Weisser, B. Romero, *et al.*, "Carrier dynamics and microwave characteristics of GaAs-based quantum-well lasers," IEEE J. Quantum Electron. **35**(4), 635–646 (1999).
24. R. S. Tucker and D. J. Pope, "Microwave Circuit Models of Semiconductor Injection Lasers," IEEE Trans. Microwave Theory Techn. **31**(3), 289–294 (1983).
25. X. Li, Z. Ghassemlooy, S. Zvanovec, *et al.*, "An Equivalent Circuit Model of a Commercial LED With an ESD Protection Component for VLC," IEEE Photon. Technol. Lett. **33**(15), 777–779 (2021).
26. W. N. Cheung, P. J. Edwards, and G. N. French, "Determination of LED equivalent circuits using network analyser measurements," in *1998 Conference on Optoelectronic and Microelectronic Materials and Devices. Proceedings (Cat. No.98EX140)*, (1998), 232–235.
27. X. Li, Z. Ghassemlooy, S. Zvanovec, *et al.*, "Equivalent Circuit Model of High Power LEDs for VLC Systems," in *2019 2nd West Asian Colloquium on Optical Wireless Communications (WACOWC)*, 2019), 90–95.
28. I. Hino and K. Iwamoto, "LED Pulse response analysis considering the distributed CR constant in the peripheral junction," IEEE Trans. Electron Devices **26**(8), 1238–1242 (1979).
29. E. Bogatin, *Signal and Power Integrity - Simplified* (Signal and Power Integrity - Simplified, 2010).
30. X. Shan, S. Zhu, P. Qiu, *et al.*, "Multifunctional Ultraviolet-C Micro-LED With Monolithically Integrated Photodetector for Optical Wireless Communication," J. Lightwave Technol. **40**(2), 490–498 (2022).
31. Z. Yuan, Y. Li, X. Lu, *et al.*, "Investigation of Modulation Bandwidth of InGaN Green Micro-LEDs by Varying Quantum Barrier Thickness," IEEE Trans. Electron Devices **69**(8), 4298–4305 (2022).